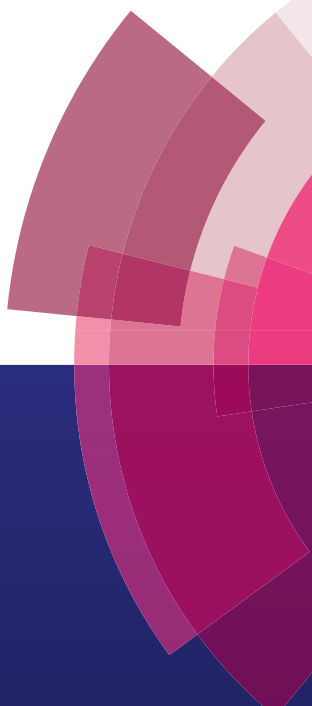
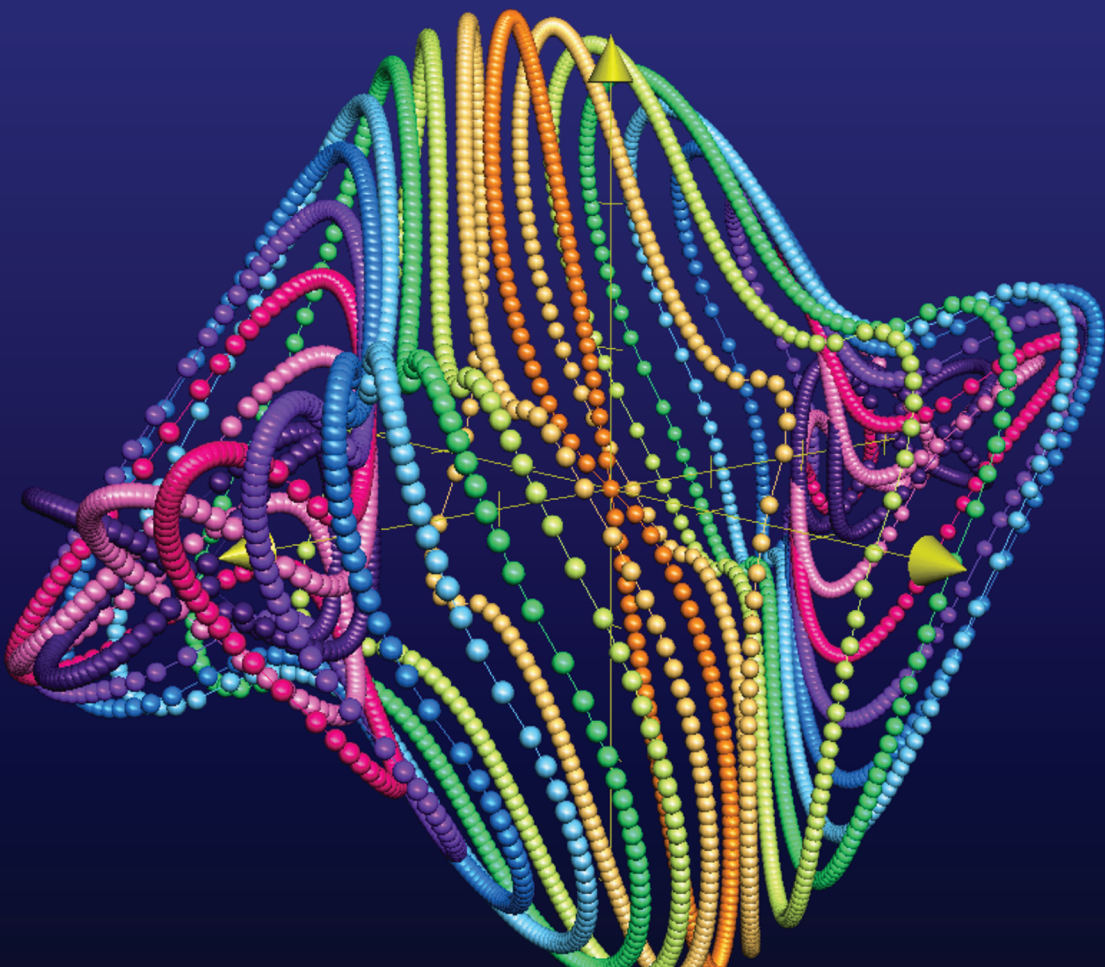
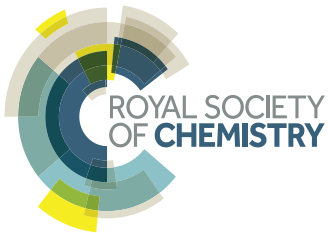


Soft Matter

www.softmatter.org



ISSN 1744-683X



PAPER

James E. Martin and Kyle J. Solis

Creating orbiting vorticity vectors in magnetic particle suspensions
through field symmetry transitions—a route to multi-axis mixing

175 YEARS



Cite this: *Soft Matter*, 2016,
12, 1021

Creating orbiting vorticity vectors in magnetic particle suspensions through field symmetry transitions—a route to multi-axis mixing

James E. Martin* and Kyle J. Solis

It has recently been reported that two types of triaxial electric or magnetic fields can drive vorticity in dielectric or magnetic particle suspensions, respectively. The first type—symmetry-breaking rational fields—consists of three mutually orthogonal fields, two alternating and one dc, and the second type—rational triads—consists of three mutually orthogonal alternating fields. In each case it can be shown through experiment and theory that the fluid vorticity vector is parallel to one of the three field components. For any given set of field frequencies this axis is invariant, but the sign and magnitude of the vorticity (at constant field strength) can be controlled by the phase angles of the alternating components and, at least for some symmetry-breaking rational fields, the direction of the dc field. In short, the locus of possible vorticity vectors is a 1-d set that is symmetric about zero and is along a field direction. In this paper we show that continuous, 3-d control of the vorticity vector is possible by progressively transitioning the field symmetry by applying a dc bias along one of the principal axes. Such biased rational triads are a combination of symmetry-breaking rational fields and rational triads. A surprising aspect of these transitions is that the locus of possible vorticity vectors for any given field bias is extremely complex, encompassing all three spatial dimensions. As a result, the evolution of a vorticity vector as the dc bias is increased is complex, with large components occurring along unexpected directions. More remarkable are the elaborate vorticity vector orbits that occur when one or more of the field frequencies are detuned. These orbits provide the basis for highly effective mixing strategies wherein the vorticity axis periodically explores a range of orientations and magnitudes.

Received 7th August 2015,
Accepted 27th October 2015

DOI: 10.1039/c5sm01975c

www.rsc.org/softmatter

1 Introduction

In this paper we demonstrate that it is possible to use symmetry transitions between certain classes of alternating triaxial magnetic fields to produce time-dependent, noncontact, multi-axial stirring in fluids containing small volume fractions of magnetic particles. In this approach to mixing, the vorticity axis continuously changes its direction and magnitude, executing elaborate, periodic orbits through all three spatial dimensions. These orbits can be varied over a wide range by phase-modulating one or more field components, and a wide variety of orbits can be created by controlling the phase offset between the field components. The results in this paper constitute an entirely new approach to efficient mixing and heat transfer in complex geometries.

Mixing with triaxial magnetic fields has some unique and attractive characteristics.^{1,2} Only a small volume fraction of magnetic particles is needed ($\sim 1\text{--}2$ vol%); only modest,

uniform fields (~ 150 Oe) are required; the mixing torque is independent of field frequency and fluid viscosity (within limits); and the mixing torque is independent of particle size, making this technique suitable for use in a variety of systems ranging in size from the micro to industrial scale. Furthermore, the torque density is uniform throughout the fluid, creating a ‘vortex fluid’ capable of peculiar dynamics. Finally, unlike traditional magnetic stir bars, which can experience instabilities that result in fibrillation or stagnation, there are no such instabilities associated with this technique, making it a simple, robust means of creating noncontact mixing.

This approach to mixing can eliminate or reduce the fluid stagnation that can occur in conventional stirring, in which the stirring axis is stationary. Fluid stagnation is a problem in simple geometries, such as near the interior edges of a cylindrical volume,^{3,4} and is even worse in complex or obstructed volumes, such as those that occur in engineered microfluidic systems. Moreover, in a single-axis, rotary mixing scheme, the fluid flow profile is typically non-uniform and assumes the form of an irrotational vortex,⁵ wherein the fluid velocity is inversely proportional to the radial distance from the mixing axis.

Sandia National Laboratories, Nanomaterials Sciences, Albuquerque, New Mexico, USA 87185. E-mail: jmartin@sandia.gov

This work on inducing flow in bulk liquids complements advances in liquid surface mixing using magnetic particles driven by an alternating magnetic field.^{6–9} In this approach the field organizes the particles into complex aggregations, such as “snakes,” and the induced motion of these aggregations creates significant near-surface vorticity. These surface mixing techniques share an important similarity with the bulk mixing techniques we have pursued: viscosity as a means of control. In the surface flow experiments increasing the viscosity causes a transition from the formation of “snakes” to the formation of asters,” which have less vigorous flow.¹⁰ When we increase the liquid viscosity in our suspensions there is a transition from inducing vorticity to creating static particle aggregations.

1.1 Background

In the last few years it has been shown that a wide variety of triaxial magnetic fields can produce strong fluid vorticity.^{11–13} These fields are comprised of three mutually orthogonal field components, of which either two or three are alternating, and whose various frequency ratios are rational numbers. These dynamic fields generally lack circulation, in that a magnetically soft ferromagnetic rod subjected to one of these fields does not undergo a net rotation during a field cycle. Yet these fields do induce deterministic vorticity, which might seem counterintuitive. For this deterministic vorticity to occur it must be reversible. This reversibility is possible if the trajectory of the field and its physically equivalent converse, considered jointly, is reversible. This field parity occurs because the symmetry of this union of fields is shared by vorticity, which is reversible.

An analysis of the symmetry of these fields enables the prediction of the vorticity axis, which is determined solely by the relative frequencies of the triaxial field components. For these fields changing the relative phases of the components enables control of the magnitude and sign of the vorticity—and in some cases changing the sign of the dc field also reverses flow—but not the axis around which vorticity occurs. Thus, when the frequency of one of the field components is detuned slightly to cause a slow phase modulation, the vorticity will periodically reverse, but it remains fixed around a single axis. Such flows produce a simple form of periodic stirring, as occurs in a washing machine. The vorticity orbits presented in this paper go well beyond this simple form of stirring and are based on transitions in the symmetry of the triaxial field, as discussed in the following section.

2 Field-symmetry transitions

Understanding the rationale for investigating field-symmetry transitions requires a little more background. We have discovered two methods of inducing fluid vorticity in magnetic particle suspensions. In the first method two orthogonal ac components whose frequency ratio is a simple rational number are applied to the suspension. Vorticity is induced when an

orthogonal dc field is applied, because this field creates the parity required for deterministic vorticity. We have developed a theory of these Symmetry-Breaking Fields that predicts the direction and sign of vorticity as functions of the frequencies and phase.¹² The second method is based on Rational Triad Fields, comprised of three orthogonal ac fields whose frequency ratios are rational numbers (e.g., 1:2:3). These fields also have the parity and symmetry required to induce deterministic vorticity and we have developed a symmetry theory that allows us to compute the direction and sign of vorticity as functions of the frequencies and phases.¹³ In this paper we show that by progressively biasing one particular ac component of a rational triad to dc we can generate competing symmetries that lead to a continuous reorientation of the vorticity vector, providing full 3-d control of fluid vorticity.

This symmetry-transition approach is based on the observation that both ac/ac/dc (symmetry-breaking) and ac/ac/ac (rational triad) fields can generate fluid vorticity. The axis around which this vorticity occurs is the critical factor for the concept of field-symmetry-driven vorticity transitions. For the ac/ac/dc fields the vorticity axis is determined by the reduced ratio $l:m$ of the two ac frequencies. Because l and m are relatively prime then at least one of these numbers is odd. A consideration of the symmetry of the field trajectory and its equivalent converse jointly shows that if only one of these numbers is odd the vorticity is parallel to the odd field component and reversing the dc field reverses the vorticity. If both of these numbers are odd the vorticity is parallel to the dc field component. For odd:odd fields reversing the dc field direction does not reverse the flow, which suggests that for these fields the dc component can be replaced by an ac field and vorticity can still occur (the truth is a little more complicated—see discussion below). In all cases the sign and magnitude of the vorticity can be controlled by the phase angle between the two ac components.¹¹

For the fully alternating rational triads the direction of vorticity is controlled by the three relative field frequencies $l:m:n$, where l , m , and n are integers having no common factors. There are four classes of such fields: (I) even:odd:odd; (II) even:even:odd where even:even can be factored to even:odd; (III) even:even:odd where even:even can be factored to odd:odd and; (IV) odd:odd:odd.¹³ (Note that the order of the even and odd field components is of no consequence, so no distinction is made between even:even:odd and even:odd:even, etc.) By analyzing the symmetries of the 3-d Lissajous trajectories of the field and its converse jointly it is possible to show that the direction of vorticity is parallel to the field component that has unique numerical parity. The fourth class (odd:odd:odd) has no component with a unique numerical parity and so does not possess the symmetry required to predict a vorticity axis. However, we have shown that off-axis vorticity exists.¹⁴

Consider now the possibility of creating a continuous symmetry transition by gradually dc biasing one of the three ac field components of a rational triad, while keeping the root-mean-square (rms) field amplitude constant. To be definite we will let l , m , and n lie along the x , y , and z components, respectively.

If it is desired to transition the z component of the field to dc the relevant expression is

$$\begin{aligned} H_0^{-1}\mathbf{H}_0(t) &= \sin(l \times 2\pi ft + \phi_l)\hat{\mathbf{x}} + \sin(m \times 2\pi ft + \phi_m)\hat{\mathbf{y}} \\ &+ \left[\sqrt{1 - c^2} \sin(n \times 2\pi ft + \phi_n) + \frac{c}{\sqrt{2}} \right] \hat{\mathbf{z}} \end{aligned} \quad (1)$$

where f is a characteristic frequency determined by the experimentalist and ϕ_l, ϕ_m, ϕ_n are the phase angles for the three field components, which can be selected in the function generators. Note that all three field components have equal rms values and the ac-to-dc transition is effected by increasing c from 0 to 1 or from 0 to -1 . The z axis ac and dc fields have equal rms amplitudes when $c = 1/\sqrt{2}$. The effect of this ac-dc transition on field symmetry depends on both the class of rational triad as well as the component that is transitioned.

2.1 Even, odd, odd fields

To be definite we consider the odd : even : odd field 1 : 2 : 3, which is shown in Fig. 1 (left) for one particular set of phases. For this class of fields the vorticity axis is along the even direction, which is the y axis. If the y field component is continuously transitioned to dc the vorticity axis will remain in the y direction (see the symmetry-derived rules given above), so no rotation of the vorticity axis is anticipated because field symmetry is preserved in this transition. In this particular case the sign of the final vorticity is independent of the sign of the dc field, but is dependent on the phase angles of the ac field components, so a vorticity-reversal transition should be possible wherein the fluid stagnates at some value of c . Transitioning either of the odd field components to dc is much more interesting. If the x component is fully transitioned to dc a change of field symmetry occurs that causes the vorticity vector to reorient from the y to the z axis. The progression of this symmetry change can be seen in Fig. 1. For intermediate values of the dc amplitude ($0 < |c| < 1$) the field and its converse do not exhibit the symmetry of vorticity, but the continuous nature of the field transition suggests a

continuous reorientation of the vorticity axis nevertheless: it would seem unphysical for the vorticity to abruptly change at some intermediate dc field amplitude. An interesting aspect of this particular field transition is that the final vorticity sign is dependent on the dc field direction. This means there are four possible vorticity axis transitions: one wherein the vorticity axis vector transitions from $+y$ to $+z$, one from $+y$ to $-z$, one from $-y$ to $-z$ and one from $-y$ to $+z$. It is reasonable to assume that the vorticity vector rotates in the y - z plane in all cases, but we will find that this is not the case and in fact a strong vorticity component can emerge along the x axis for intermediate dc amplitudes. This unexpected out-of-plane vorticity is investigated below by using the torque density functional to compute the torque density for these fields.

The same general considerations hold when the z component is continuously transitioned to dc, only in this case the final vorticity axis is along x . In this case we expect to be able to orient the vorticity vector anywhere in the x - y plane, but a strong contribution to the vorticity occurs around the z axis, which is surprising.

To summarize, for even, odd, odd fields applying a dc bias along one odd ac component causes the vorticity to rotate from the even component direction to the other odd component. But applying a dc bias along the even component does not cause a change in the vorticity direction. The 1 : 2 : 3 field is the only field exhaustively studied in this paper, but it is interesting to consider the expected behavior of the other field classes.

2.2 Odd, even, even fields where even:even factors to odd:even

The simplest field of this class is 1 : 2 : 4. For these fields the vorticity is around the odd axis, which is x in this case. As a result, if the y or z component of the field is transitioned to dc the direction of the vorticity will not change. The sign of the vorticity might change, however, because in this case it is dependent on the sign of the dc field. Thus a symmetry-driven transition that gives rise to flow reversal can be effected by a proper selection of the dc field sign.

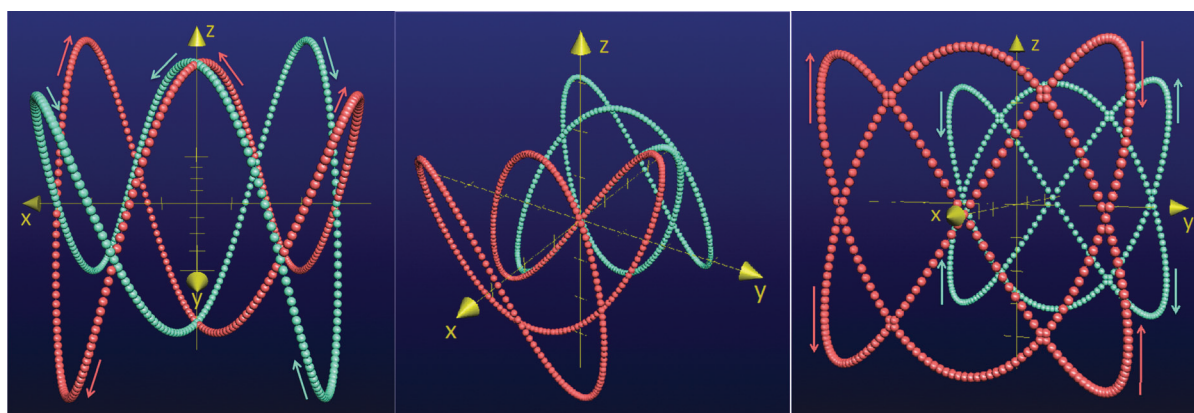


Fig. 1 The field symmetry transition is illustrated for the 1 + dc : 2 : 3 triaxial field. In the left plot the field trajectory and its converse are shown with zero dc bias. The C_2 symmetry axis of this rational triad is the y axis, which is the vorticity axis. The x and z axes are antisymmetric under a 180° rotation. The middle plot has a 50% dc bias along the x axis and does not possess the symmetry of vorticity. The right plot has 100% dc bias, so the ac amplitude is zero. This is now a symmetry-breaking rational field and the z axis is the C_2 symmetry axis and the vorticity direction.

If the x component transitions to dc the vorticity axis will reorient from the x to the y axis, with the vorticity sign again dependent on the dc field sign. In this case it is expected that the vorticity vector can be continuously oriented in the x - y plane, but the torque density functional described below predicts a surprising component along the z axis during this transition.

In summary, for odd, even, even fields applying a dc field along either even component will not change the orientation of the vorticity axis, but might cause it to reverse. Applying a dc field along the odd component will cause the vorticity to reorient from the odd field axis to the odd axis that arises from factoring even:even.

2.3 Odd, even, even fields where even:even factors to odd:odd

For this class of fields, such as 1:2:6, the vorticity is around the odd field axis, which in this case is along x . If one component of such an odd:even:even field is fully transitioned to dc there are three possible outcomes: dc:odd:odd, odd:dc:even, odd:even:dc. In each case the symmetry rules show that the vorticity is around the x axis (underlined). Therefore no change in the orientation of the vorticity is expected, though its sign and magnitude might change during the transition. In other words, such fields produce robust vorticity that is not strongly affected by stray dc fields. Note that only if an even field is transitioned does the final vorticity sign depend on the sign of the dc field.

2.4 Odd:odd:odd fields

The final case of odd:odd:odd fields is interesting because any field component that is transitioned to dc becomes the vorticity axis. This suggests that applying a dominant dc field in any direction along any field component will induce vorticity around that component, enabling facile control of the vorticity direction.

3 Predictions from the torque density functional

In a recent paper¹⁴ we proposed a measure of the torque density produced in a magnetic particle suspension subjected to a triaxial field that is based on both theory and experiment. This functional was found to conform to all of the predictions of the symmetry theories but can also be applied to those cases where the trajectories of the triaxial fields do not possess the symmetry of vorticity, such as the field-symmetry-driven vorticity transitions that are the focus of this paper. This functional also makes useful quantitative predictions for the amplitude of the torque density as a function of field frequencies and phases. The functional is given by

$$\mathbf{J}_{\{\phi\}} = \int_0^1 \mathbf{J}_{\{\phi\}}(s) ds \text{ where } \mathbf{J}_{\{\phi\}}(s) = |\mathbf{h}(s)|^2 \frac{\mathbf{h}(s) \times \dot{\mathbf{h}}(s)}{|\mathbf{h}(s) \times \dot{\mathbf{h}}(s)|} \quad (2)$$

where the dependence on the phase angles is indicated. Here $\mathbf{J}_{\{\phi\}}(s)$ is the instantaneous torque density, $\mathbf{h}(s) = H_0^{-1}\mathbf{H}_0(s)$ is the reduced field, and $s = ft$ is the reduced time in terms of the

characteristic field frequency in eqn (1). The experimentally measured, time-average torque density is related to this functional by $\mathbf{T}_{\{\phi\}} = \text{const} \times \phi_p \mu_0 H_0^2 \mathbf{J}_{\{\phi\}}$, where μ_0 is the vacuum permeability and ϕ_p is the particle volume fraction.

Before giving the predictions of the torque density functional it is informative to consider what one might reasonably expect to occur. Returning to our example case of a 1 + dc : 2 : 3 field, for zero dc field the vorticity is parallel to the y axis (along the “2” field component) and for the full dc case, dc : 2 : 3, it is parallel to the z axis, both in accordance with symmetry theory. For intermediate values of c a simple ‘rule of mixing’ consistent with a field-squared effect is

$$\mathbf{J}_{\{\phi\}}(c) = (1 - c^2) |\mathbf{J}_{\{\phi\}}(0)| \hat{\mathbf{y}} + c^2 |\mathbf{J}_{\{\phi\}}(1)| \hat{\mathbf{z}}. \quad (3)$$

This expression confines the vorticity vector to the y - z plane, which seems reasonable, but how does this expression compare to the predictions of eqn (2)? It is clear that inserting eqn (1) into eqn (2) does not result in an expression in which the ac and dc terms are separable, but it is not clear how important this is.

3.1 Predicted torque densities along the three field components

To obtain an appreciation for the complexity of this symmetry transition we have plotted in Fig. 2 components of the torque density computed from eqn (2) as functions of the phase angles ϕ_1 and ϕ_3 for $c = 0.5$. It is surprising to see that there is a component along the x axis, and in fact this is the dominant component, with a maximum value of 0.16 (arb. units) as compared to 0.09 for the y axis and 0.12 for the z axis.

One aspect of the nature of the vorticity transition from the rational triad 1:2:3 to the symmetry-breaking rational field dc : 2 : 3 is illustrated in Fig. 3, which shows the torque density for each point of a square lattice of points in the ϕ_1 - ϕ_3 plane, separated by 10° along each cardinal direction. For the rational triad ($c = 0$) the computed torque vectors are along the y axis, so changing the phase angles merely changes the magnitude and sign of the vorticity. But even when a small dc bias is applied along the x axis the torque vectors have comparable components along both the x and z axes. Changing the phase angles thus enables a change in both the magnitude and direction of the fluid vorticity through all three dimensions. As the dc field increases, the locus of torque densities expands, eventually attaining a shape reminiscent of a pendulum ride at a fair. This locus finally collapses onto the z axis when the field along the x axis no longer contains an ac component: this is the symmetry-breaking-field limit, where $c = 1$.

The full range of 3-d control of the torque density is given in Fig. 4, where torque density data for numerous values of the dc bias are plotted, again for the square lattice of phase angles referred to in Fig. 3. The torque density has significant components in the x and z directions and by proper selection of the dc bias and phase angles vorticity can be created along essentially any direction. This complex set of vorticity vectors has implications for non-stationary flow, as we will see.

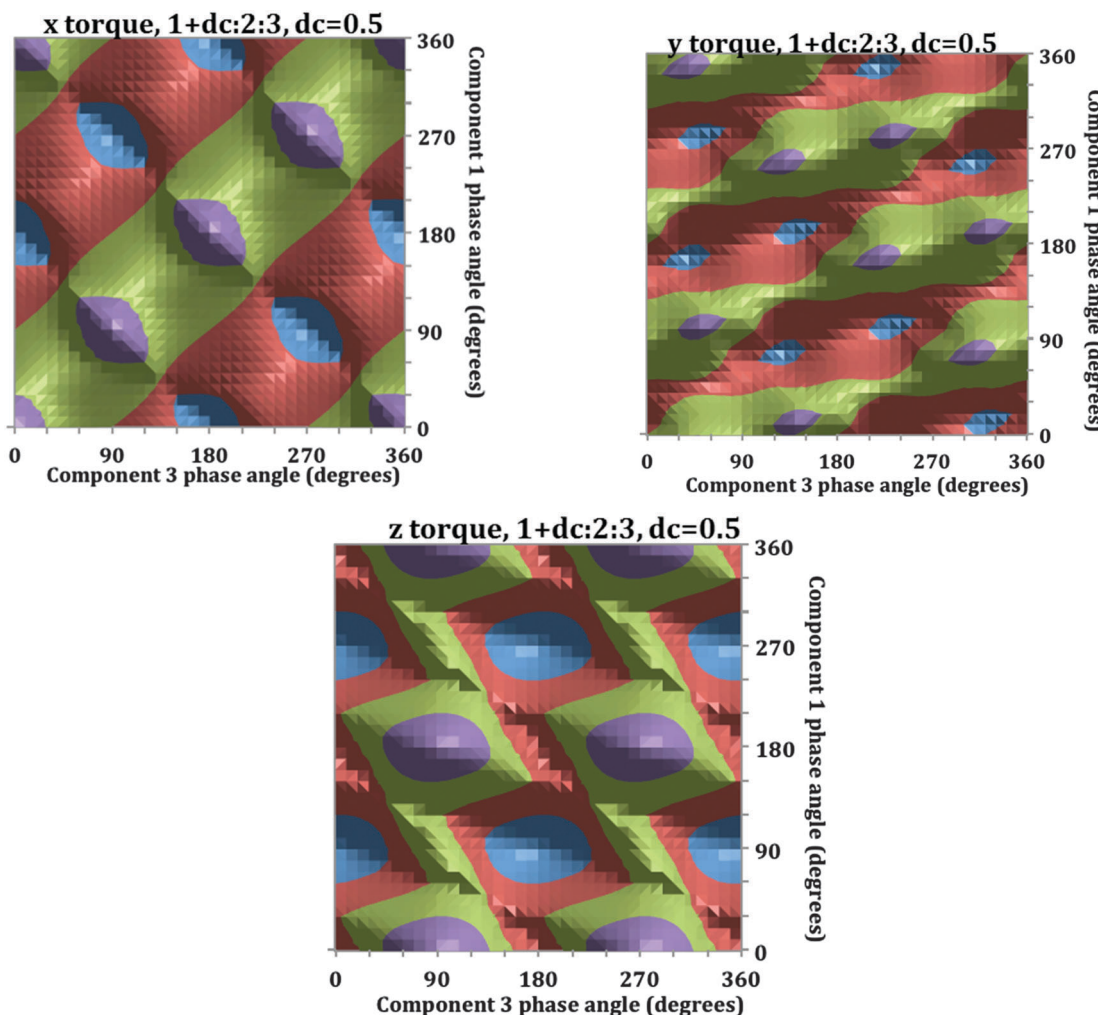


Fig. 2 Predicted torque components along all three axes for a $1 + dc : 2 : 3$ field with $c = 0.5$.

It is interesting to determine how the torque density produced at any given pair of phase angles evolves as the dc bias is progressively increased. To this purpose we have investigated phase angles along the first three transects shown in Fig. 5. This figure serves as the color key for the curves in Fig. 6. Recall that each of these curves must start on the y axis and terminate on the z axis.

Fig. 6 (top left) shows the result of using the simple mixing law of eqn (3) to estimate the torque density during the field symmetry transition from $1:2:3$ to $dc:2:3$. The only inputs into this mixing law are the computed y axis torque densities for $c = 0$ and the z axis torque densities for $c = 1$. Here each line represents a different pair of phase angles along the first transect shown in Fig. 5. For this transect $\phi_1 = 0^\circ$ and ϕ_3 increases from 0° to 360° by intervals of 20° . Not all colors in the key are shown because certain phase angles give the same curves when this mixing law is used. Equivalent ϕ_3 angles are $(90^\circ + n, 90^\circ - n)$ and $(270^\circ + n, 270^\circ - n)$ where $0^\circ \leq n \leq 90^\circ$. Data are for $0 \leq c \leq 1$ in intervals of 0.01. This mixing law predicts that the torques are confined to the y - z plane, but the behavior predicted by the torque functional is much richer.

When the functional in eqn (2) is used to predict the torque density the result is dramatically different. Fig. 6 (top right) shows computations for the phase angles along the first transect. All the colors in the key in Fig. 5 are now shown because each pair of phase angles produces a unique curve. These torque density curves have substantial deviations from the y - z plane and in some cases the x torque component even dominates. In all cases if the dc field is reversed ($0 \geq c \geq -1$) both the x and the z torque components are reversed, which constitutes a rotation by 180° around the y axis. Torque density calculations for points along the second and third transects are also given in Fig. 6. Once again, the x component of the torque often dominates. Reversing the dc field ($0 \geq c \geq -1$) would fill out the upper hemisphere for torque densities along the second transect, but would do nothing along the third transect. We conclude that, in general, increasing the dc bias is expected to produce a complex evolution of the vorticity.

3.2 The prediction of vorticity orbits

Phase modulating components of the applied $1 + dc : 2 : 3$ field produces a rich variety of vorticity orbits that are both interesting

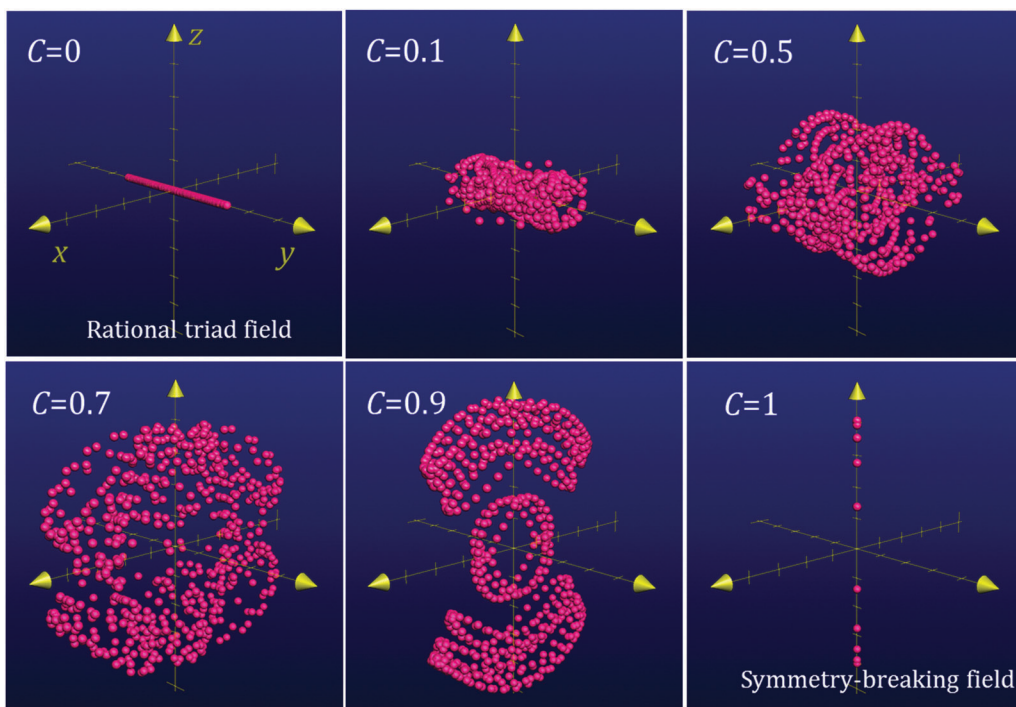


Fig. 3 The nature of the continuous vorticity transition from the rational triad $1:2:3$ to the symmetry-breaking rational field $dc:2:3$ is illustrated. These data are the computed torque functional, eqn (2), for a square lattice of points in the $\phi_1-\phi_3$ plane in Fig. 2, separated by 10° along each cardinal direction. For the rational triad ($c = 0$) the computed torque vectors are along the y axis, so changing the phase angles merely changes the magnitude. When a dc bias is applied along the x axis the torque vectors fairly explode off the y axis to have significant components along both the x and z axes, so changing the phase angles now enables a change in both the magnitude and direction of the fluid vorticity. As the dc field increases, this cloud of torque density data expands into a shape reminiscent of a pendulum ride, finally collapsing onto the z axis when the field along the x axis no longer contains an ac component: this is the symmetry-breaking-field limit, where $c = 1$. Field biasing thus enables continuous control over the direction of the vorticity direction. The tick marks on all axes are separated by 0.025. Note that there are the same number of data points in each plot, but these become degenerate in the $c = 1$ plot. The approach to degeneracy can be seen in the $c = 0.9$ plot.

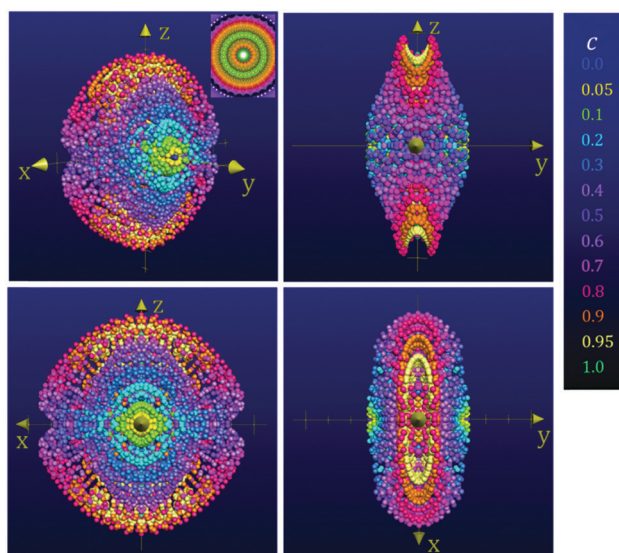


Fig. 4 The data in Fig. 3 are presented, along with other values of the relative dc field amplitude, so that the full range of vorticity control can be appreciated. The maximum torque density amplitude in the x direction is roughly equal to that of the z direction. The tick marks on all axes are separated by 0.025 and each axis ranges from -0.28 to 0.28 . Inset is a mandala that seems to capture the appearance of the data.

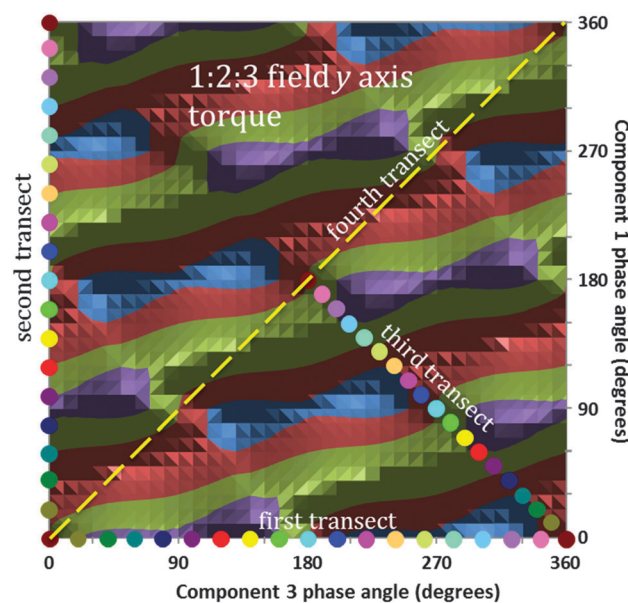


Fig. 5 The torque component along y for a $1:2:3$ field is shown along with the color keys for the first, second, and third transects used to generate Fig. 6.

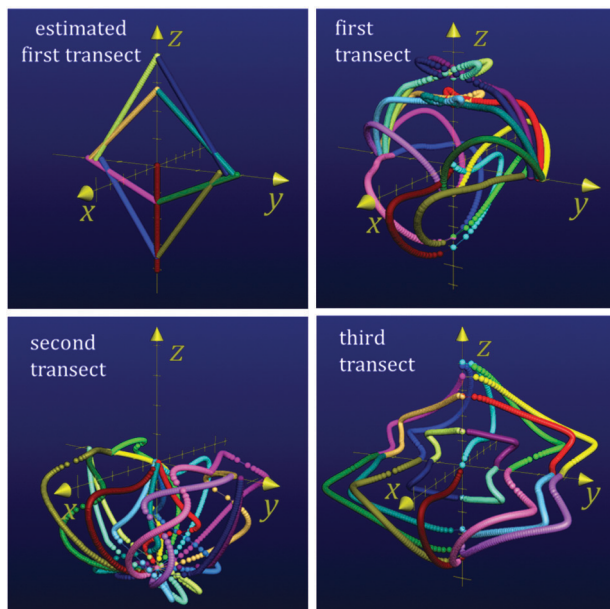


Fig. 6 (top left) The result of using eqn (3) to estimate the torque density during the transition from 1:2:3 to dc:2:3. Each line represents a different set of phase angles along the first transect shown in Fig. 5. For this transect $\phi_1 = 0^\circ$ and ϕ_3 increases from 0° to 360° by intervals of 20° . Not all colors in the key are shown because certain phase angles give the same curves. Equivalent ϕ_3 angles are $(90^\circ + n, 90^\circ - n)$ and $(270^\circ + n, 270^\circ - n)$ where $0^\circ \leq n \leq 90^\circ$. Data are for $0 \leq c \leq 1$ in intervals of 0.01. The torques start on the y axis and end on the z axis and are confined to the y - z plane. The tick marks on all axes are separated by 0.025. (top right) When the torque functional in eqn (2) is used to predict the torque density for points along the first transect the result is dramatically different than the simple rule of mixing. All the colors in the key in Fig. 5 are shown because each point gives a unique curve. These torque curves have substantial deviations from the y - z plane: in some cases the x torque is dominant. If the dc field is reversed ($0 \geq c \geq -1$) both the x and the z components of the torque are reversed. (bottom left & right) Torque functional calculations for points along the second and third transects during the transition from 1:2:3 to dc:2:3, respectively. The key for the colors is given in Fig. 5. Again, in some cases the x torque dominates. If the dc field component is reversed ($0 \geq c \geq -1$) both the x and the z components of the torque are reversed, which would fill out the upper hemisphere for second transect, but do nothing for the third transect.

and potentially useful for a number of applications. We have numerically investigated these orbits for the dc bias $c = 0.5$. In Fig. 7 are shown the simplest possible vorticity orbits, taken along the four transects shown in Fig. 5. In the laboratory the first transect would be realized by slightly detuning the field frequency along the z axis. The second transect would be obtained by detuning the frequency of the x component. The third transect requires detuning both of these field components by equal and opposite amounts, and for the fourth transect by equal amounts.

The fourth transect is a bit of a disappointment, as the torque density barely changes, but the other transects produce striking results. The first and second transects produce orbits with a net torque around the z axis (averaged over one orbital cycle) but with zero net torques around the other axes. For these orbits the mixing is persistent. The orbit for the third transect is interesting in that it produces zero net torque around any of the

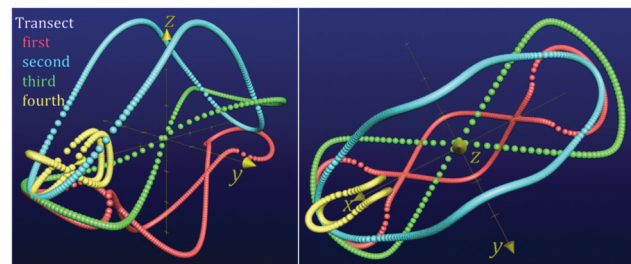


Fig. 7 Field heterodyning produces strange vorticity orbits. In this case the heterodyne paths are simply along the transects shown in Fig. 5. Along the first transect only the z component frequency is detuned and along the second transect only the x field component is detuned. For the third transect both the x and z components are detuned by equal and opposite amounts. For the fourth transect the x and z components are detuned by equal amounts. This heterodyning produces persistent vorticity of ever-changing direction, except for along the third transect, where the torque density does vanish. Along the fourth transect heterodyning accomplishes little. These orbits were computed for the case where the rms ac and dc components are equal, $c = 0.5$.

principal axes, which would enable complex mixing in free-standing droplets without incurring any net migration of the droplet. This mixing strategy would be ideal for the development of parallel bioassays of container-less droplet arrays, perhaps comprised of millions of droplets. The fourth transect produces a non-zero net torque around the x axis alone.

The phenomenology of these vorticity orbits is much richer than indicated, Fig. 7 being only the tip of the iceberg. Fig. 8 shows the effect of adding a phase offset to one of the field components, in this case the x component, to create transects that are parallel to those already discussed. The left figure shows a family of orbits obtained by transects parallel to the fourth transect in Fig. 5. This set of orbits was obtained by adding phases from 0 – 180° in increments of 10° . The rather confined vorticity orbit in Fig. 7 grows into large orbits and finally collapses back into the tiny fish-shaped orbit at a phase shift of 180° , but reflected in the y - z plane.

The same phase shifts were used to generate a set of orbits for a set of transects parallel to the second transect, generating the set of widely varying vorticity orbits in the right plot of Fig. 8. Adjustment of the relative phase enables a great deal of control over the dynamics of the vorticity vector induced by biased rational triad fields.

Finally, we briefly investigated vorticity orbits for a few cases where the field frequencies along the x and z axes are detuned by unequal amounts, specifically by $2:1$. These orbits, shown in Fig. 9, are really elaborate. One can only imagine the complexity that would emerge if we applied phase shifts to these transects. But the situation is bad enough already, so we did not pursue this topic further. The question at this point is whether or not these vorticity orbits actually exist. After all, the torque density functional is merely an ansatz.

4 Experimental setup

The magnetic particle suspension consisted of molybdenum-Permalloy platelets $\sim 50\ \mu\text{m}$ across by $0.4\ \mu\text{m}$ thick

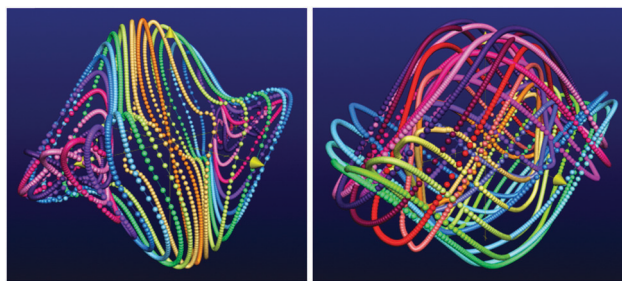


Fig. 8 The heterodyne orbits are sensitive to the relative phase, which provides a simple means of orbit control. The left orbits are for heterodyne transects parallel to transect four in Fig. 5. Changing from one orbit to another requires only a change of the phase on a signal generator. The right orbits are for heterodyne transects parallel to the second transect in Fig. 5.

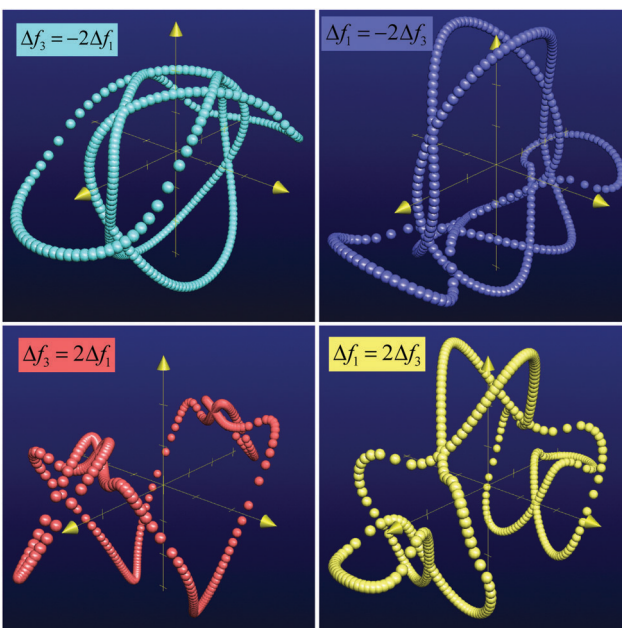


Fig. 9 Elaborate vorticity vector orbits occur when the field components are detuned by different amounts. Here we consider four simple cases that arise when the x and z field components are detuned by a ratio of 2 : 1. Inset into each plot is the relative frequency detunings used to generate these orbits. Referring to eqn (1) the top left orbit corresponds to $\phi_1 = \Delta f_1$ and $\phi_3 = -2\Delta f_1$, where $\Delta f \ll f$. Adding a constant phase shift to either field component will alter these orbits. The point is that heterodyning can produce complex variations in the magnitude and direction of the vorticity vector.

(Novamet Corp.) dispersed into isopropyl alcohol at a low volume fraction.

For the 1 : 2 : 3 rational triad field studied in this work the fundamental frequency was 36 Hz (f in eqn (1)) and all three field components were 150 Oe (rms). The spatially uniform triaxial ac magnetic fields were produced by three orthogonally-nested Helmholtz coils. Two of these were operated in series resonance with computer-controlled fractal capacitor banks.¹⁵ The third coil was driven directly in voltage mode by a Kepco bi-polar operational power supply/amplifier (BOP 36-12M). The phase shift of this coil at its operational frequency of 36 Hz was measured as +68° with a precision LCR meter (Agilent 4284A).

To compensate for this phase shift we added this phase to the signal that drives the Kepco amplifier.

The signals for the three field components were produced by two phase-locked Agilent/HP function generators (equipped with option 005), allowing for stable and accurate control of the phase angle of each field component. Note that if these signals are simply produced from separate signal generators there will be a very slow phase modulation between the components due to the finite difference in the oscillator frequency of each function generator. And simply running two separate signal generators off the same oscillator does not control their phase relation. Because all of our measurements are strongly dependent on phase, option 005 is necessary.

To quantify the magnitude of the vorticity, the torque density of the suspension was computed from measured angular displacements on a custom-built torsion balance (see ref. 12 for a picture). A 1.5 vol% suspension was contained in a small vial (1.8 mL) attached at the end of the torsion balance and suspended into the central cavity of the Helmholtz coils *via* a 96.0 cm-long, 0.75 mm-diameter nylon fiber with a torsion constant of $\sim 13 \mu\text{N m rad}^{-1}$.

5 Results and discussion

5.1 Locus of torque density vectors

All of the above predictions depend on one key point: the appearance of torque along the x axis when a dc field is applied parallel to this axis. Recall that this torque does not exist for $c = 0$ or 1, but is only expected for intermediate values, *i.e.*, during the symmetry transition. In fact, upon the application of the dc bias this torque does appear, and is strong, which came as no small relief. Fig. 10 shows the measured torque density along each of the three field components for the 1 + dc : 2 : 3 biased triaxial field with $c = 0.7$, where both the ac and dc contributions of the biased field component have nearly equal rms amplitudes. These experimental data were taken for a square lattice of points in the phase angle plane of Fig. 5 on 10° intervals, so in each of these three plots there are $36 \times 36 = 1296$ data points. However, the symmetry of the data reduces the required number of measurements for each plot to a fourth of this, 324.

The set of measured vorticity vectors is plotted in Fig. 11 (left). These data can be compared to the computed data for the corresponding value of $c = 0.7$ in Fig. 3. The detailed appearance is different, but the essential point is that the locus of points does not simply lie in the y - z plane, but has significant components along the x axis. In fact, the maximum specific torque density (torque density divided by the volume fraction of particles) along the x axis is 476 J m^{-3} , which can be compared to the maxima of 1127 and 993 J m^{-3} along the y and z axes, respectively. These torque maxima were obtained for a balanced 1 + dc : 2 : 3 biased triad with $c = 0.7$, where each field component had equal rms amplitudes. We also varied only the dc field amplitude (at fixed ac field amplitudes corresponding to $c = 0.7$) to see if this had any effect on the torque maxima. The torque maximum along the y axis is maximized for a dc field corresponding

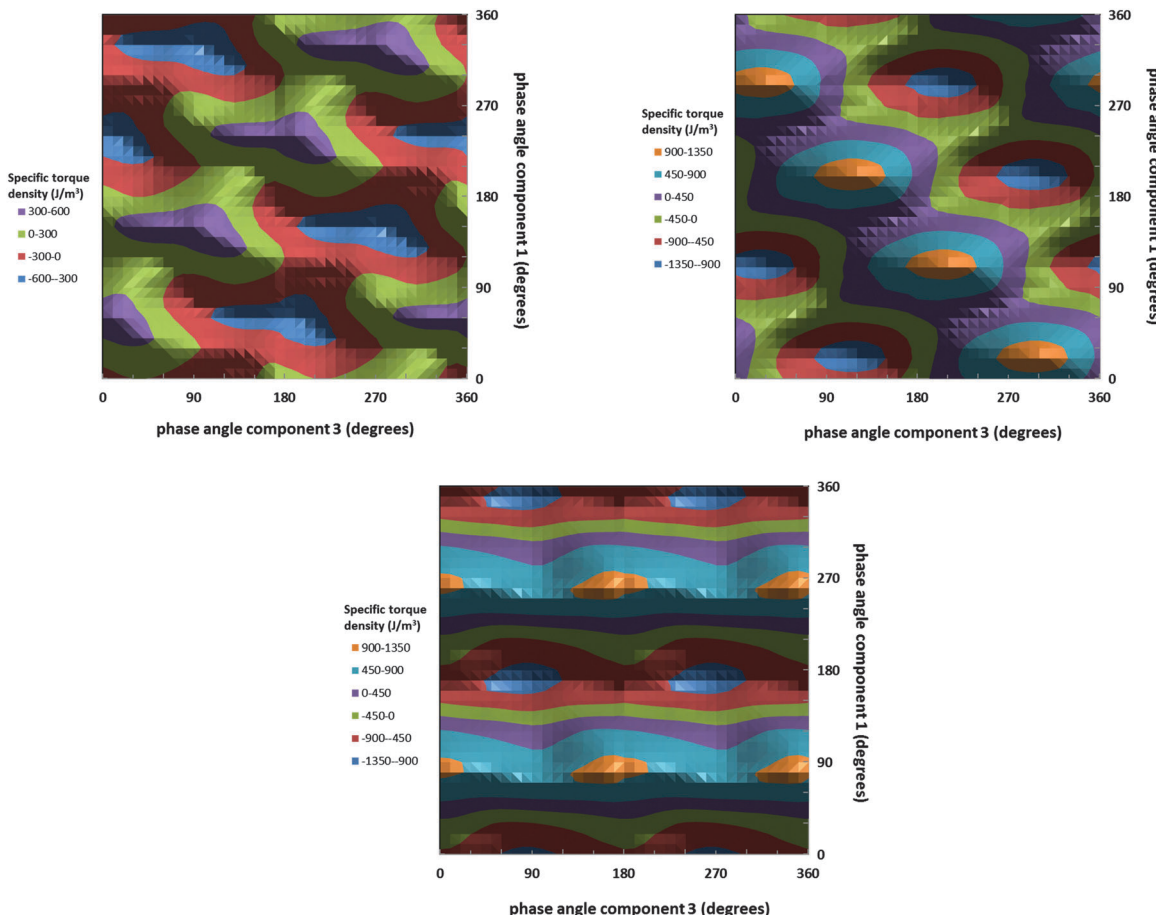


Fig. 10 Experimental torque density plots for the x (top left), y (top right) and z (bottom) torque components. These data are for the $1 + dc : 2 : 3$ field with $c = 0.7$.

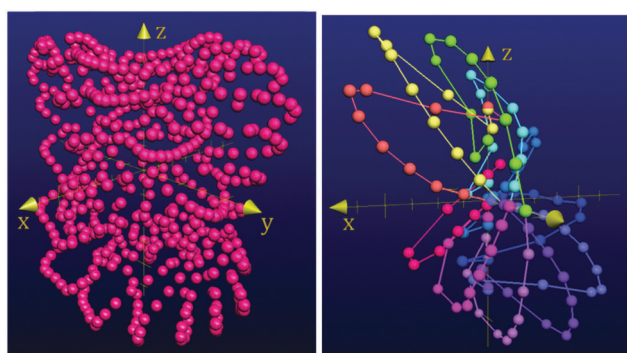


Fig. 11 (left) The locus of possible vorticity vectors for the $1 + dc : 2 : 3$ biased rational triad with $c = 0.7$. These points span all three spatial dimensions, indicating that complex vorticity orbits can exist. (right) The evolution of the vorticity vectors taken along the third transect as c is increased from 0 to 1. Each colored curve is for a different set of phase angles. Each curve starts on the y axis and terminates on the z axis. The important feature is the large torque density amplitude along the x axis.

to $c = 0.7$, but the x and z axis torques increased modestly to 602 and 1215 J m^{-3} by decreasing the dc field by $\sim 33\%$ and 24% respectively. Phase modulating can be expected to create three-dimensional orbits that intersect these points.

The progression of the measured torque density as the dc field is increased from $c = 0$ to 1 is shown in Fig. 11 (right) for points taken along the third transect of Fig. 5, but with a phase offset of $+60^\circ$ applied to the x axis (36 Hz) component, to ensure a significant torque density around this axis [see Fig. 10 (top left)]. These curves start on the y axis and terminate on the z axis and although they differ from the computed curves for the third transect, Fig. 6 (bottom right), they do share the characteristic of being symmetric under a 180° rotation around the y axis. Again, the essential point is that these curves are substantially different than the reasonable prediction given in eqn (3) in that they are not confined to the y - z plane.

5.2 Vorticity orbits

The vorticity orbits can be obtained by detuning one or more field components. To be clear about the experimental parameters the field can be written

$$\begin{aligned} H_0^{-1}\mathbf{H}_0(t) &= \sin[2\pi(f_1 + \Delta f_1)t + \phi_1]\hat{\mathbf{x}} + \sin(2\pi f_2 t)\hat{\mathbf{y}} \\ &\quad + \frac{1}{\sqrt{2}} \left[\sin[2\pi(f_3 + \Delta f_3)t] + \frac{1}{\sqrt{2}} \right] \hat{\mathbf{z}} \end{aligned} \quad (4)$$

where $f_1 = f$, $f_2 = 2f$ and $f_3 = 3f$. We have included the parameters Δf_1 and Δf_3 to indicate detuning of the first and third field

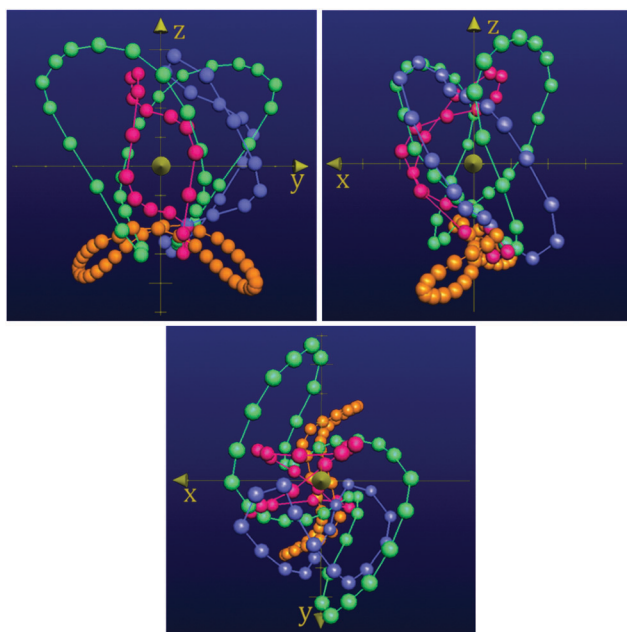


Fig. 12 Experimental vorticity orbits along the four transects shown in Fig. 5 are viewed along each field component. Transect one is depicted in orange, transect two in green, transect three in violet, transect four in red. When averaged over a cycle, transects one and two have a net z axis vorticity, transect four has a net x axis vorticity, and transect three has a net y axis vorticity, in substantial concurrence with the predictions from the torque density functional in Fig. 7.

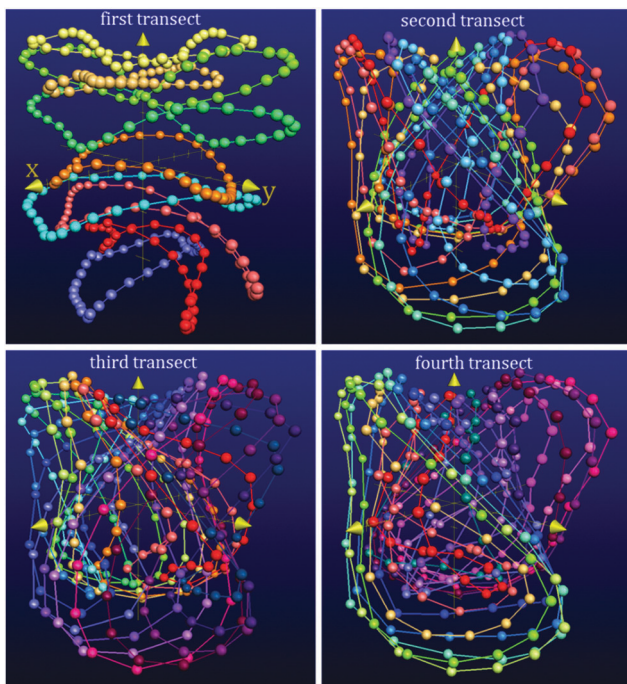


Fig. 13 Phase offsets significantly alter the vorticity orbits in Fig. 12 obtained for each of the four transects shown in Fig. 5. For transects parallel to each of the principal transects in Fig. 5, but offset by successive intervals of 20° , we can construct a succession of vorticity orbits that can be obtained by simply selecting the corresponding phase offsets on the signal generators (see eqn (4)). Considerable tuning of the orbits is possible from a push of a button.

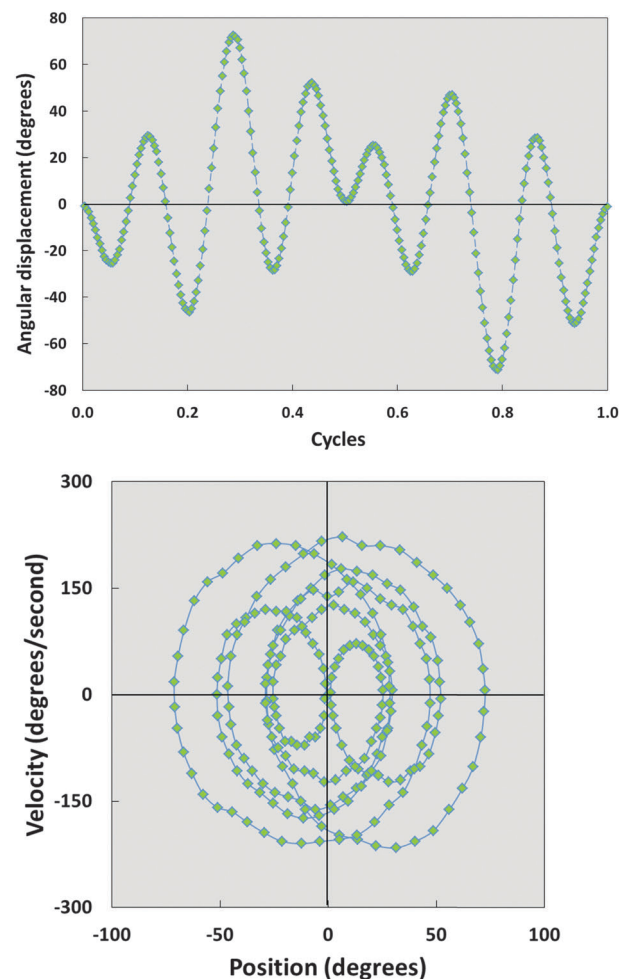


Fig. 14 For the phase modulated $1 + dc : 2 : 3$ with $c = 0.7$, given by the frequencies 36.1, 72 and 108.2 Hz the x axis torque is plotted as a function of cycles (top) and versus the time derivative of the torque (bottom) to make a phase plot. The torque is periodic, though not a simple sinusoid, and the phase plot indicates a strongly non-harmonic dynamics, since it is not a simple ellipse.

components. The principal vorticity orbits for the $1 + dc : 2 : 3$ field, in Fig. 12, are for zero offset phase, *i.e.*, $\phi_1 = 0$, and correspond to the four transects in Fig. 5, which are $\Delta f_1 = 0$, $\Delta f_3 = \text{const}$; $\Delta f_1 = \text{const}$, $\Delta f_3 = 0$; $\Delta f_3 = -\Delta f_1$; and $\Delta f_3 = \Delta f_1$, respectively. In Fig. 13 are shown the families of orbits that emerge when the offset phase is increased from 0 to 340° by 20° intervals. Note that many of the points are the same in these plots, since they must be comprised of the available data points in Fig. 11 (left), but the orbits interconnect these points in different ways.

The complexity of these orbits can be appreciated by one single phase modulation example, wherein we monitored the x component of the torque for the frequencies 36.1, 72 and 108.2 Hz and recorded the torque density as a function of time. The time dependence of this single component of the vorticity orbit is plotted in Fig. 14 (top), which shows a periodic behaviour that is not a simple sinusoid. The phase plot in Fig. 14 (bottom) shows strongly non-harmonic dynamics, since harmonic dynamics yield an ellipse. For this particular circumstance the variations

in the torque density are symmetric about zero, indicating zero time-averaged vorticity, but there are many phase modulation cases where the vorticity never changes sign. In general, the phase plots can be very complex.

6 Conclusions

We have shown that applying a dc field parallel to a carefully chosen alternating component of an ac/ac/ac rational triad field can create a field-symmetry transition. By exploiting this transition we have shown through computation and experiment that the vorticity vector can be oriented in a wide range of directions that comprise all three spatial dimensions. The direction of the vorticity vector can be controlled by the relative phases of the field components and the magnitude of the dc field. Detuning one or more field components to create phase modulation causes the vorticity vector to trace out complex orbits of a wide variety, creating robust multiaxial stirring. This multiaxial, noncontact stirring is attractive for applications where the fluid volume has complex boundaries, or is congested. Multiaxial stirring would be an effective way to deal with the dead zones that can occur when stirring around a single axis and could eliminate the accumulation of particulates that frequently occurs in such mixing. But beyond the practical implications of this new technology there is a great deal of interesting science. A future challenge is a first-principles, microscopic theory of the dynamics of particles in these fields that would enable accurate predictions of the vorticity orbits and the other phenomena we have observed.

Acknowledgements

Sandia National Laboratories is a multi-program laboratory managed and operated by Sandia Corporation, a wholly owned subsidiary of Lockheed Martin Corporation, for the U.S. Department of Energy's National Nuclear Security Administration under contract DE-AC04-94AL85000. This work was supported by Jerry Simmons *via* the Laboratory-Directed Research and Development (LDRD) office at Sandia National Laboratories. We thank Matt Groo at Novamet for supplying the magnetic platelets.

References

- 1 J. E. Martin, Theory of strong intrinsic mixing in vortex magnetic fields, *Phys. Rev. E: Stat., Nonlinear, Soft Matter Phys.*, 2009, **79**, 011503.
- 2 J. E. Martin, L. Shea-Rohwer and K. J. Solis, Strong intrinsic mixing in vortex magnetic fields, *Phys. Rev. E: Stat., Nonlinear, Soft Matter Phys.*, 2009, **80**, 016312.
- 3 C. Gualtieri, Numerical simulation of flow and tracer transport in a disinfection contact tank, Third Biennial Meeting: International Congress on Environmental Modelling and Software (iEMSS), 2006.
- 4 S. Suresh and S. Sundaramoorthy, *Green Chemical Engineering: An introduction to catalysis, kinetics, and chemical processes*, CRC Press, USA, 2014.
- 5 S. Kay, *An introduction to fluid mechanics and heat transfer*, The Syndics of the Cambridge University Press, New York, USA, 2nd edn, 1963.
- 6 G. Kokot, A. Snezhko and I. S. Aranson, Emergent coherent states and flow rectification in active magnetic colloidal monolayers, *Soft Matter*, 2013, **9**, 6757–6760.
- 7 A. Snezhko, Non-equilibrium magnetic colloidal dispersions at liquid-air interfaces: dynamic patterns, magnetic order and self-assembled swimmers, *J. Phys.: Condens. Matter*, 2011, **23**, 153101.
- 8 M. Belkin, A. Snezhko, I. S. Aranson and W.-K. Kwok, Driven magnetic particles on a fluid surface: Pattern assisted surface flows, *Phys. Rev. Lett.*, 2007, **99**, 158301.
- 9 M. Belkin, A. Glatz, A. Snezhko and I. S. Aranson, Model for dynamic self-assembled magnetic surface structures, *Phys. Rev. E: Stat., Nonlinear, Soft Matter Phys.*, 2010, **82**, 015301.
- 10 P. L. Piet, A. V. Straube, A. Snezhko and I. S. Aranson, Viscosity control of dynamic self-assembly in ferromagnetic suspensions, *Phys. Rev. Lett.*, 2013, **110**, 198001.
- 11 J. E. Martin and K. J. Solis, Symmetry-breaking magnetic fields create a vortex fluid that exhibits a negative viscosity, active wetting, and strong mixing, *Soft Matter*, 2014, **10**, 3993–4002.
- 12 K. J. Solis and J. E. Martin, Torque density measurements on vortex fluids produced by symmetry-breaking rational magnetic fields, *Soft Matter*, 2014, **10**, 6139–6146.
- 13 J. E. Martin and K. J. Solis, Fully alternating, triaxial electric or magnetic fields offer new routes to fluid vorticity, *Soft Matter*, 2015, **11**, 241–254.
- 14 J. E. Martin and K. J. Solis, Quantifying vorticity in magnetic particle suspensions driven by symmetric and asymmetric multiaxial fields, *Soft Matter*, 2015, **11**, 7130–7142.
- 15 J. E. Martin, A resonant biaxial Helmholtz coil employing a fractal capacitor bank, *Rev. Sci. Instrum.*, 2013, **84**, 094704.